Electron Transport Dynamics in a Room-Temperature Au Nanoparticle Molten Salt

Wei Wang, Dongil Lee,† and Royce W. Murray*

Kenan Laboratories of Chemistry, University of North Carolina at Chapel Hill, Chapel Hill, North Carolina 27599-3290

Received: January 27, 2006; In Final Form: March 22, 2006

A room-temperature Au_{38} nanoparticle polyether melt has been prepared by exchanging poly(ethylene glycol) (PEG) thiolate ligands, HS−C6−PEG_{163}, into the organic protecting monolayer of $Au_{38}(PhC2)_{24}$ nanoparticles. Spectral and electrochemical properties verify that the Au_{38} core size is preserved during the exchange. Adding $LiClO_4$ electrolyte, free PEG plasticizer, and/or partitioned CO_2 leads to an ionically conductive nanoparticle melt, on which voltammetric, chronoamperometric, and impedance measurements have been made, respectively, of the rates of electron and ion transport in the melt. Electron transport occurs by electron self-exchange reactions, or electron hopping, between diffusively relatively immobile Au_{38}^0 and Au_{38}^{1+} nanoparticles. The rates of physical diffusion of electrolyte ions (diffusion coefficients D_{CION}) are obtained from ionic conductivities. The measured rates of electron and of electrolyte ion transport are very similar, as are their thermal activation energy barriers, observations that are consistent with a recently introduced ion atmosphere relaxation model describing control of electron transfer in semisolid ion and electron-conductive media. The model has been previously demonstrated using a variety of metal complex polyether melts; the present results extend it to electron transfers between Au nanoparticles. In ion atmosphere relaxation control, measured rates and energy barriers for electron transfer are not intrinsic values but are instead characteristic of competition between back-electron transfer caused by a Coulombic disequilibrium resulting from an electron transfer and relaxation of counterions around donor−acceptor reaction partners so as to reachieve local electroneutrality.

Introduction

Our previous studies of highly concentrated redox moieties in viscous, amorphous media have focused on a basic understanding of their electrochemistry and electron transport dynamics, which would play a role in their application as energy storage materials.[1] A number of chemical materials—from metal complexes[2] to organic entities[3] to DNA[4]—have been transformed into room-temperature amorphous molten salts by judicious covalent attachments of poly(ethylene) glycol (PEG) oligomers to, for example, metal complex ligands (e.g., bipyridine[2], tetraphenylporphyrin[5]) or to their counterions.[3b,6] This route to generation of molecular melts has proved to be completely general and works by disrupting normally crystalline structures with disordered PEG appendages, forming glassy or semisolid media consisting of concentrated redox sites diluted only modestly by the PEG component. In the electrochemical reactions of these media, as examined by microelectrode methodologies,[7] the combination of high redox site concentrations and their very slow physical diffusivities engenders electron transport by electron hopping. These have proved to be excellent model media for the study of electron transport in semisolid, localized redox site materials.[2−6,8]

Our initial analysis of electron transport in redox melts focused on a solvent dynamics interpretation.[9] An improved more recent analysis is based on the experimentally strong linkage of the electron transfer reaction to its local ionic environment.[8] The high concentration of electron donor−acceptor sites in redox melts leads to an intrinsically strong electrostatic association between cations and anions. The sluggish mobility of counterions surrounding (even less mobile) electron donor−acceptor reaction partners enhances the unfavorable Coulombic charge separation that is created by an electron transfer between those partners. The charge separation becomes compensated by either a redistribution of counterions surrounding the reaction partners or back-electron transfer. Because the charge-diffusive mode of electron transport measurement that we employ is insensitive to the latter and reflects only the rate of charge transport fruitful counterion redistribution, the electrochemical measurement is capable of uncovering this form of electron transfer rate control.

Evidence for the coupling of electron transport to counterion mobility extends over a wide range of PEG-based molten salts.[4,8,10] For example, for cobalt and ruthenium complex molten salts, the results demonstrate (a) a 1:1 proportionality between counterion diffusion coefficient and both heterogeneous (e.g., Co(III/II)[8c]) and homogeneous (e.g., Co(II/I),[8a,b] Ru(III/II)[8d,e]) electron transfer rates, (b) very similar thermal energy barriers for electron transport and counterion diffusion, and (c) electron transport rates that fall to effectively zero when the counterion (e.g., DNA[4]) is immobile. Substantial effort has been put into structural variations of metal complex molten salts in terms of metals (Co, Ru), counterions (ClO_4^- or I^-),[8e] PEG linkage (to cation or anion),[8b,c] number of PEG chains,[8d,e] supporting electrolyte addition,[8d] and CO_2 plasticization.[8a,b] All of these examples have entailed more or less conventional redox materials, and all have shown adherence to the ion atmosphere relaxation analysis. It is with interest in exploring the *generality* of ion atmosphere relaxation in electron hopping transport that

* Author to whom correspondence should be addressed. E-mail: rwm@unc.edu.

† Present address: Department of Chemistry, Western Michigan University, Kalamazoo, MI 49008.

10.1021/jp060598i CCC: $33.50
Published on Web 05/10/2006

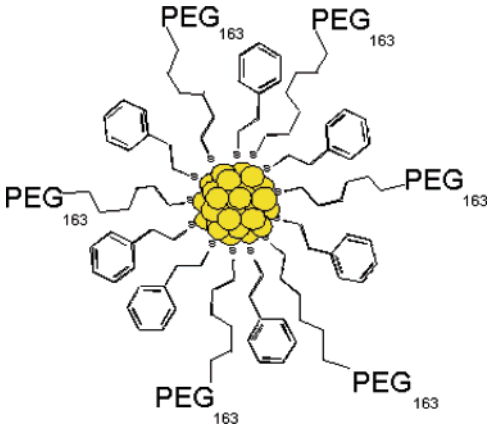

Figure 1. Cartoon of the structure of $Au_{38}(PhC2)_{15}(SC6PEG_{163})_9$.

in this paper we turn to less conventional redox reactions, namely, electron transfer between molecule-like Au nanoparticles.

This work describes molten salts based on 1.1 nm diameter Au_{38} thiolate monolayer-protected nanoparticles. These nanoparticles are part of a family of nanoparticles within which over a 1−3 nm range of core diameters properties[11] change from those of bulk Au (or at least Au particles that lack a highest occupied molecular orbital (HOMO)−lowest unoccupied molecular orbital (LUMO) energy gap) to those that exhibit such a gap. The Au_{38} nanoparticles, or monolayer-protected clusters (MPCs), with phenylethanthiolate ligand monolayers and an estimated $Au_{38}(PhC2)_{24}$ formula, display in dilute dichloromethane solutions cleanly defined voltammetric one-electron oxidation and reduction transformations[12] that are separated by 1.6 V. After correction for charging energy, the estimated HOMO−LUMO gap energy is ca. 1.3 eV, which is confirmed by optical band edge measurement.[12c] While this molecule-like behavior justifies treatment as a redox moiety, the electron transfer dynamics between tiny clumps of metal atoms remain a novel area of chemistry.

The above-mentioned energy gap properties are preserved upon exchange of some of the original phenylethyl thiolate ligands with thiolated PEG ligands.[13] Our tactic to prepare a molecular melt of Au_{38} nanoparticles relies on the successful melt-generation ideas noted above[2−6,8] of attaching poly(ethylene) glycol chains. In this case, the poly(ethylene) glycol chains are attached as thiolate ligands to produce a highly viscous, room-temperature melt in which the melt components are PEGylated nanoparticles as illustrated in Figure 1. Electrolyte ($LiClO_4$) is dissolved in the nanoparticle phase (much as in a polymer electrolyte[14]) along with some unattached PEG to make the melt ionically conductive enough to allow microelectrode voltammetry in the otherwise undiluted material. The PEGylated ligand in Figure 1 is $-S-C6-PEG_{163}$ (or $-S(CH_2)_6-(OCH_2CH_2)_3OCH_3$). (It differs from that used previously,[12b] $-SPEG_{350}$ where PEG 350 is monomethyl poly(ethylene glycol) with a molecular weight of 350 Da and an average of 7.2 repeat units. Inclusion of the hexane segment and use of a shorter PEG chain facilitated cleanup[15] of the synthesized thiol ligand.)

The electron hopping dynamics between Au_{38}^0 and Au_{38}^{1+} nanoparticles and the mass transport properties of electrolyte ions were studied at room temperature and below in the resulting Au_{38} nanoparticle melts. The electron transport rates were measured by potential step chronoamperometry of the $Au_{38}^{1+/0}$ voltammetric wave; the electron diffusion coefficient (D_E) is converted to apparent electron self-exchange rate constants (k_{EX}). Ionic conductivities were measured by alternating current (AC) impedance and converted to physical diffusion coefficients of perchlorate ions (D_{ClON}) with the Nernst−Einstein relation. The thermal activation barrier energies of each were obtained by varying temperatures. Further manipulation of overall melt fluidity, and of transport rates, was accomplished by plasticization by sorption of high-pressure CO_2. These measurements follow those used previously.[2−6,8]

The resulting values of D_E and of D_{ClON} vary in a nearly 1:1 manner, and their thermal barrier energies are very similar. These results show that ion atmosphere relaxation can control the effective rate of electron transport in a semisolid nanoparticle phase, just as it does in the well-studied metal complex molten salts.

Experimental Section

Chemicals. All chemicals were reagent grade and used as received if not otherwise stated.

Poly(ethylene glycol) methyl ether (molecular weights of 350 and 550 Da) was dried in a vacuum oven at 75 °C for at least 3 days before use. $Au_{38}(PhC2)_{24}$ nanoparticles were prepared as described previously.[12a]

Syntheses. The PEGylated thiol (1-mercaptohex-6-yl)tri(ethylene glycol) methyl ether ($HSC6PEG_{163}$) was prepared by procedures similar to that reported by Whitesides et al.[16] as described in the Supporting Information.

Preparation of PEGylated Au_{38} Melts. $HSC6PEG_{163}$ was incorporated into the monolayer of Au_{38} nanoparticles by ligand exchange. In a typical procedure, 17 mg of $Au_{38}(PhC2)_{24}$ was stirred in the dark with 3 equiv of $HSC6PEG_{163}$ (32 mg) in 10 mL of methylene chloride for 24 h. Concentrating the reaction mixture by rotary evaporation gave a dark-red oil that was washed several times with *n*-heptane to remove free thiol as shown by the absence of their α-thiol proton resonances in ^1H NMR. The relative proportion of PEGylated and PhC2 thiolates in the resulting mixed monolayer was determined by decomposing the Au_{38} nanoparticle with a crystal of iodine, analyzing the liberated mixture of disulfides[17] by ^1H NMR.

Free methyl-terminated PEG (molecular weights of 350 or 550 Da) plasticizer and $LiClO_4$ electrolyte were added to the resulting mixed monolayer $Au_{38}(PhC2)_{15}(SC6PEG_{163})_9$ melt by dissolving all in acetonitrile,[18] mixing thoroughly, and evaporating the solvent. PEG plasticizers were added in at least 5:1 molar chain proportions, relative to the $-SC6PEG_{163}$ ligands. $LiClO_4$ electrolyte was added at a typical 1:16 Li^+/ether oxygen molar ratio, or a little above 1 M concentration in the dried melt.[9b] While the electrolyte concentration was held relatively constant, its concentration relative to MPCs varied by as much as a factor of 3-fold, owing to plasticizer content.

Measurements. ^1H NMR spectra were collected on a Bruker 500 MHz DRX spectrometer and referenced to deuteronmethylene chloride (D, 99.9%, Cambridge Isotope Laboratories, Inc.)

Voltammetry in dilute CH_2Cl_2 or CH_3CN solutions (with 0.1 M Bu_4NPF_6 electrolyte) and in undiluted polyether melts of nanoparticles was done with a CHI 660A electrochemical workstation. Voltammetry in degassed dilute solutions used a 1.6 mm diameter Pt disk working electrode and Ag wire quasi-reference and Pt coil counter electrodes. Voltammetry was executed on films of Au_{38} polyether melts with added $LiClO_4$ on a polished, insulating platform in which tips of two Pt (12.5 μm radius as working and 0.4 mm diameter as counter electrode) and one Ag (0.5 mm diameter quasi-reference electrode (QRE)) wires were exposed. A second 0.4 mm diameter Pt wire tip was also present in the platform and was used with the other

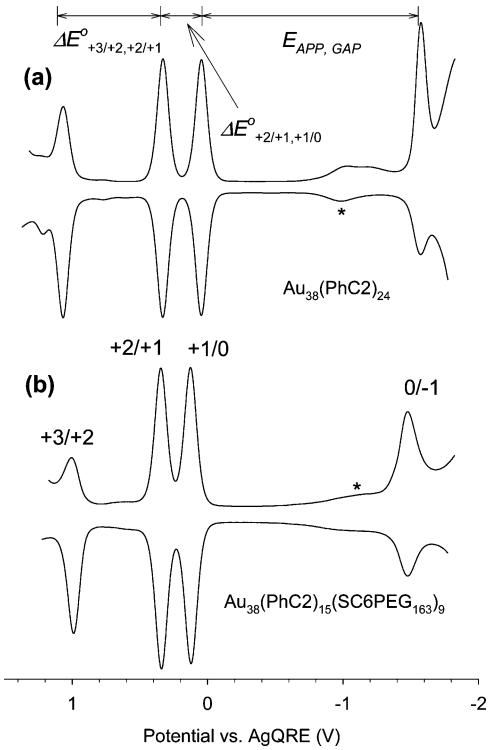

Figure 2. Differential pulse voltammograms of (a) $Au_{38}(PhC2)_{24}$ in methylene chloride and (b) $Au_{38}(PhC2)_{15}(SC6PEG163)_9$ in acetonitrile with 0.1 M Bu_4NPF_6 as the supporting electrolyte, at a 1.6 mm diameter Pt disk working electrode. Potential scan rate = 0.02 V/s. The star indicates currents from residual dioxygen.

0.4 mm tip during ionic conductivity measurements. The platform was polished with successively smaller grades (down to 0.05 μm) of alumina, and the Pt tips were electrochemically cleaned by cycling in 0.1 M H_2SO_4.[19] The film of the nanoparticle melt was drop-cast onto the electrode platform to a thickness at about 1 mm and dried in vacuo (ca. 1×10^{-3} Torr) for 24 h. The electrochemistry was also performed in vacuo, and the films and cell enclosure were preequilibrated at each temperature and pressure for at least 2 h. Chronoamperometric potential steps (300−500 mV) were guided by initial cyclic voltammetric scans and started in a non-Faradaic region just before the $Au_{38}^{1+/0}$ wave to a diffusion-limited potential past the $Au_{38}^{1+/0}$ peak (but short of the $Au_{38}^{2+/1+}$ reaction). The current−time results were analyzed by the Cottrell equation.[7]

Ionic conductivities of nanoparticle melts (with added $LiClO_4$) were measured by AC impedance using a Solartron Model SI 1260 impedance/gain phase analyzer SI 1287 electrochemical interface combination, over a 1−500 kHz frequency range, at 0 V direct current (DC) bias and 50 mV amplitude. Ionic conductivity was calculated as the ratio of the geometric cell constant (calibrated by standard solutions) and the cell resistance taken from the low-frequency real-axis intercept of the complex impedance semicircle.

Results and Discussion

Ligand Exchange. The nanoparticle melts used here have been prepared by ligand exchange of the PEGylated thiol $HSC6PEG_{163}$ with the well-characterized[12] nanoparticle $Au_{38}(PhC2)_{24}$. It is of course important that the Au_{38} core remain intact through the exchange procedure. This has been shown to be the case for Au_{38} in other studies,[12,13] and confirming electrochemical and spectral evidence is presented next.

Figure 2 compares dilute solution differential pulse voltammetry (DPV) of the ligand-exchanged product, $Au_{38}(PhC2)_{15}(SC6PEG_{163})_9$, with that of the original nanoparticle $Au_{38}(PhC2)_{24}$. The pattern of redox changes for $Au_{38}(PhC2)_{24}$ has been discussed previously;[12c] the current peaks at ca. +0.1 V vs QRE represent loss of the first electron from the Au_{38} core whereas those at ca. −1.5 V represent the first reduction step of the core. The difference between their potentials, $E_{APP,GAP}$, represents the HOMO−LUMO energy gap plus charging energy.[20] The charging energy is approximated by the difference in potential for loss of the first and second electrons ($\Delta E°_{2+/1+,1+/0}$). These data are listed in Table 1 for $Au_{38}(PhC2)_{15}(SC6PEG_{163})_9$ and $Au_{38}(PhC2)_{24}$ and for two other reported mixed monolayer Au_{38} examples.[12] It is seen that the general appearance of the Figure 2 voltammetry and the numerical results for $Au_{38}(PhC2)_{15}(SC6PEG_{163})_9$ of $E_{APP,GAP}$ and the HOMO−LUMO energy gap, 1.65 and 1.34 V, respectively, are nearly identical to those of $Au_{38}(PhC2)_{24}$ and the other nanoparticles. The small differences seen could be due to a combination of experimental uncertainty and differences between electronic inductive effects[13] of the different ligands.

The UV−vis spectra of $Au_{38}(PhC2)_{15}(SC6PEG_{163})_9$ and $Au_{38}(PhC2)_{24}$ solutions (Figure 3) are also nearly identical; three absorbance features appear in each case at 400, 445, and 680 nm, along with other minor inflections.[12a] The absorbance coefficients differ to a small degree; that of $Au_{38}(PhC2)_{15}(SC6PEG_{163})_9$ is about 10% larger at 680 nm, for example. Other data on Au_{38} nanoparticles also show small increases in the absorbance coefficient as the monolayer becomes increasingly PEGylated.[21] Overall, neither the electronic spectra nor voltammetry of the PEGylated $Au_{38}(PhC2)_{15}(SC6PEG_{163})_9$ are significantly altered from their $Au_{38}(PhC2)_{24}$ precursor. Assuming that these properties are influenced by the nanoparticle core size, the results indicate that core size changes do not occur.

Electron Charge Transport and Counterion Transport. The oxidative cyclic voltammetry of a $Au_{38}(PhC2)_{15}(SC6PEG_{163})_9$ melt containing MePEG plasticizer and 1 M $LiClO_4$ electrolyte is shown in Figure 4a at room temperature and in Figure 4b at a series of temperatures. The melt exhibits a series of oxidative features similar to those in dilute solution (Figure 2), except that the product of the third oxidation step is apparently unstable, with following chemical events leading to further electron transfer steps. The 1+/0 and 2+/1+ waves are better behaved; the former appears to be cleanly chemically reversible. The shape of the voltammetric waves indicates linear transport geometry—even though a microelectrode is employed—because of the very slow transport rates. Without the added plasticizer, the uncompensated resistance is sufficiently large as to significantly distort the voltammetry; the iR_{UNC} effect even with MePEG plasticizer present is substantial. Figure 4b shows that the peak currents for the $Au_{38}^{1+/0}$ reaction increase with temperature from −10 to 20 °C, as expected for an increase in diffusive charge transport rates. We note that although the currents are larger at higher temperature, the iR_{UNC} effect is smaller (ΔE_{PEAK} between oxidation and reduction peak currents decreases); this is because the currents increase with the square root of charge transport D_{APP}, while solution resistance scales inversely linearly with D_{APP}. At the highest temperature shown (30 °C), the reduction return wave seems smaller, suggesting an onset of thermal instability. Temperatures used for transport measurements were accordingly kept below 25 °C.

The rates of electron transport in nanoparticle melts containing different proportions of MePEG plasticizer were measured by chronoamperometry, stepping the potential over the first Au_{38} oxidation peak. In the concentrated, highly viscous melt, the

TABLE 1: Comparison of Formal Potentials (*E* vs QRE) and Spacing between Waves (V) of Various Oxidation and Reduction States of $Au_{38}(PhC2)_{24}$, $Au_{38}(PhC2)_{15}(SC6PEG_{163})_9$, $Au_{38}(PhC2)_{11}(SC6PEG_{135})_{13}$, and $Au_{38}(C6S)_{22}(PhC2S)_2$ in Methylene Chloride Containing 0.1 M Bu_4NPF_6

	potential (V)			
nanoparticle	$\Delta E°_{3+/2+,2+/1+}$[a]	$\Delta E°_{2+/1+,1+/0}$	$\Delta E°_{1+/0,1-/0}$ (=$E_{APP,GAP}$)	$[\Delta E°_{1+/0,1-/0}] - [\Delta E°_{2+/1+,1+/0}]$[b] (HOMO−LUMO gap)
$Au_{38}(PhC2)_{24}$	0.74	0.29	1.62	1.33
$Au_{38}(PhC2)_{15}(SC6PEG_{163})_9$	0.77	0.31	1.65	1.34
$Au_{38}(PhC2)_{11}(SC6PEG_{135})_{13}$	0.68	0.26	1.65	1.39
$Au_{38}(C6S)_{22}(PhC2S)_2$	0.80	0.34	1.68	1.34

[a] $\Delta E°_{3+/2+,2+/1+} = E°_{3+/2+} - E°_{2+/1+}$, the difference between the third and the second formal oxidation potentials. The other $\Delta E°$ values are analogously calculated. [b] Electrochemical HOMO−LUMO gap after the charging energy correction.

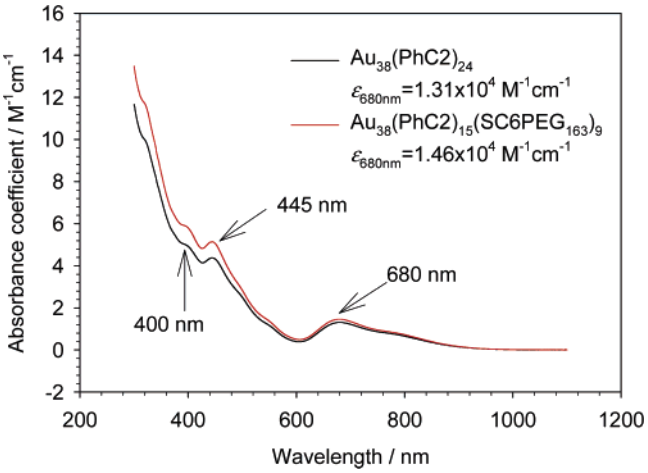

Figure 3. Comparison of UV−vis spectra of $Au_{38}(PhC2)_{15}(SC6PEG163)_9$ (black) and $Au_{38}(PhC2)_{24}$ (red) in methylene chloride. Absorbance coefficients at 680 nm are given for comparison.

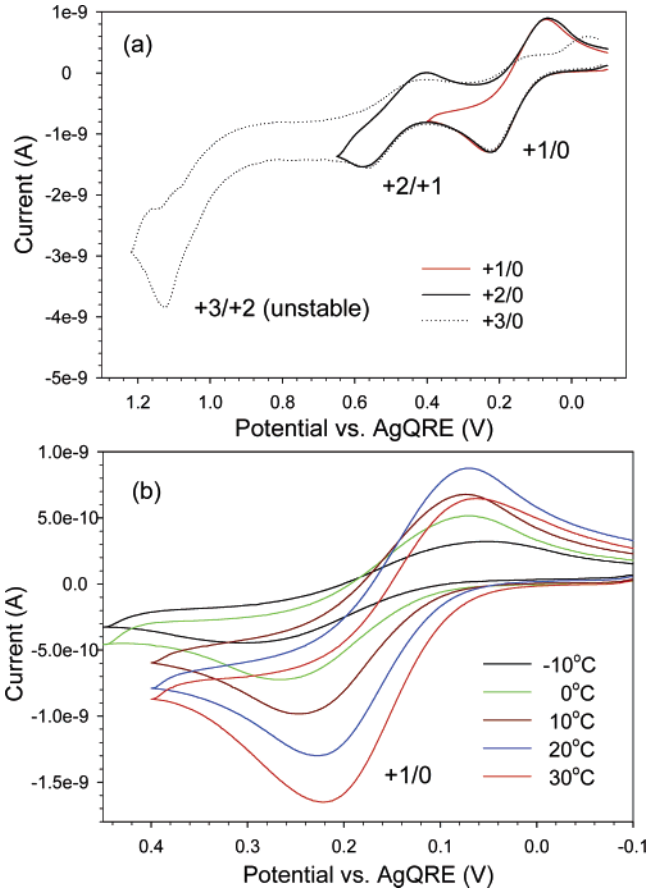

Figure 4. Cyclic voltammetry at 25 mV/s of Au_{38} polyether melts with added $MePEG_{350}$ (5:1) and 1 M $LiClO_4$ (Li^+/ether oxygen ≈ 1:16) on a 12.5 μm Pt disk microelectrode. (a) The positive-going scan variously stops beyond the first (red, −), second (black, −), and third oxidation peak (- - -), respectively. The temperature is 25 °C. (b) The scan stops beyond the first oxidation peak, and temperatures are varied from −10 to 30 °C.

apparent charge transport diffusion coefficient (D_{APP}) is expected to be a summation of the coefficients for physical diffusion (D_{PHYS}) of the $Au_{38}(PhC2)_{15}(SC6PEG_{163})_9$ moiety and for electron diffusion (D_E) by hopping between Au_{38}^0 and Au_{38}^{1+} centers in the mixed valent transport layer formed around the working electrode. The pertinent relation is known as the Dahms−Ruff equation,[22] and the value of D_E is connected to the electron self-exchange rate constant (k_{EX}) with a cubic lattice model[22]

$$D_{APP} = D_{PHYS} + D_E = D_{PHYS} + \frac{k_{EX}\delta^2 C}{6} \qquad (1)$$

where δ is the average equilibrium center-to-center distance between Au_{38} sites and C is the total concentration of redox sites.

Our experience with polyether-based molecular melts and molten salts has been that the rates of physical diffusion of bulky redox centers in the highly viscous, semisolid media are usually much smaller than D_E; i.e., $D_{APP} \approx D_E$.[2,8] In metal complex polyether melts, for example, D_{PHYS} of the PEGylated complex $[Co(bpy(MePEG_{350})_2)_3]^{2+}$ is ca. 10^{-11} cm^2 s^{-1}, but D_E for electron hopping between $[Co(bpy(MePEG_{350})_2)_3]^{2+}$ and $[Co(bpy(MePEG_{350})_2)_3]^{1+}$ is about 2 orders of magnitude larger.[8a] The apparent diffusion coefficient measured is therefore dominated by D_E with negligible contribution from D_{PHYS}. In those melts, the value of D_{PHYS} was measured from currents for the $[Co(bpy(MePEG_{350})_2)_3]^{3+/2+}$ oxidation wave. We followed a similar strategy in the nanoparticle melts, using a dilute solution of $[Co(bpy(MePEG_{350})_2)_3]^{2+}$ in the nanoparticle melt (the metal complex and Au_{38} nanoparticle have roughly the same dimensions) as a surrogate for a nonelectron hopping Au_{38} (in this case reducing the Co complex rather than oxidizing it). The results of that experiment (see Figure S-2 and the discussion in the Supporting Information) confirm that physical diffusion of the nanoparticle must also be quite slow and that the D_{PHYS} term in eq 1 can be neglected. The electron self-exchange rate constants (k_{EX}) were accordingly calculated directly from D_{APP}. The results are shown in Table 2. As expected the charge transport rates increase with added plasticizer. The results will be discussed further below.

Sorption of CO_2 at high pressure is another useful tactic to systematically[8a,b] manipulate melt fluidity to examine responses of transport rates. Sorption and the presumed increase in internal free volume have been found to enhance both electron hopping and counterion transport to degrees dependent on the CO_2 pressure.[23] Cyclic voltammetry of the Au_{38} nanoparticle melt

TABLE 2: Voltammetric Measurements of Electron Transport Rate and Ion Diffusion Measurements in Au_{38} Nanoparticle Polyether Melt (25 °C) with Added Plasticizers $MePEG_{350}$ or $MePEG_{550}$ and $LiClO_4$ Electrolyte at Li^+/Ether Oxygen ≈ 1:16[9b]

	plasticizer content[a]			
	$MePEG_{350}$		$MePEG_{550}$	
measured parameter	5:1	7.9:1[b]	5:1[b]	10:1
C_{MPC}[c]/10^{-2} M	3.90	3.14	3.14	1.74
C_{LiClO_4}[d]/M	1.04	1.17	1.17	1.27
C_{ClO_4}/C_{MPC}	27	37	37	73
$d_{core-to-core}$[e]/nm	3.49	3.75	3.75	4.57
D_{APP} (25 °C)/10^{-8} cm^2 s^{-1}	0.83	1.42	0.84	1.72
k_{EX}[f] (25 °C)/10^7 M^{-1} s^{-1}	1.05	1.92	1.15	2.84
$E_{A,ET}$[g]/kJ mol^{-1}	54 ± 1	49 ± 3	50 ± 1	63 ± 4[h]
D_{ClON}[i] (25 °C)/10^{-8} cm^2 s^{-1}	1.19	1.84	1.86	1.83
$E_{A,ClON}$/kJ mol^{-1}	54 ± 2	53 ± 4	56 ± 4	53 ± 1
a/nm (assuming $K_{eq} = 1$)	2.68	2.74	3.56	3.02
a/nm (assuming $K_{eq} = 0.1$)	0.85	0.87	1.13	0.96

[a] Plasticizer content is stated as ratio (e.g., 5:1) of moles of added $MePEG_{350}$ relative to moles of −S−C6−PEG_{163} ligands on Au_{38}. All ratios in this row share the same meaning. [b] A 7.9:1 mole ratio of added $MePEG_{350}$ is equivalent, in number of ethylene oxide groups, to a 5:1 mole ratio of $MePEG_{550}$. [c] The concentration is based on density measurements. [d] Molar concentration of $LiClO_4$. [e] Average center-to-center distance $d^3 = 1/(N_A C)$, assuming a cubic lattice model. [f] D_{PHYS} in eq 1 is presumed negligible compared to D_E. [g] From slopes of thermal activation plots of k_{EX} (for data from 25 to −10 °C). [h] This thermal barrier is under the condition of a larger core−core average separation, at higher plasticizer content. [i] Calculated from conductivity according to the Nernst−Einstein equation, assuming $D_{Li^+} \approx 0$.

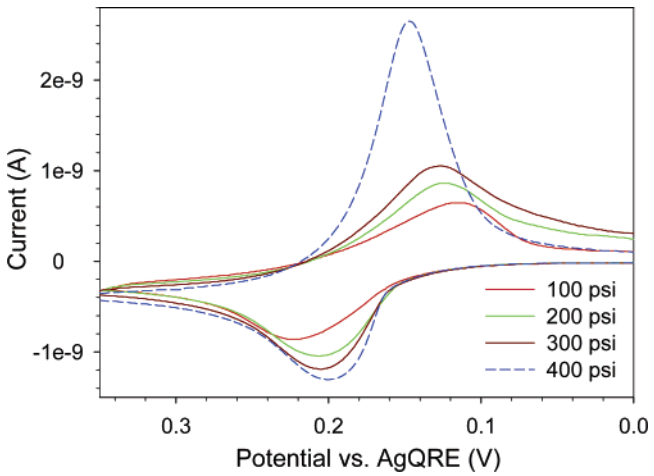

Figure 5. Cyclic voltammograms (25 mV/s) of Au_{38} polyether melts with added $MePEG_{550}$ (5:1) and 1 M $LiClO_4$ (Li^+/ether oxygen ≈ 1:16) on a 12.5 μm Pt disk electrode at 15 °C under vacuum and different CO_2 pressures.

at 25 °C is shown in Figure 5 under different CO_2 pressures. The peak currents increase with pressure, as expected, but at 400 psi there is a significant change of peak shape and an enhanced return reduction wave, suggesting that transport of oxidized Au_{38} states away from the electrode interface has somehow been greatly slowed. Higher pressures were accordingly not employed. Charge transport rates in the CO_2-plasticized melts were measured using chronoamperometry, and the k_{EX} results[24] (again taking $D_{APP} \approx D_E$) are given in Table 3. The charge transport rates for both MePEG and CO_2-plasticized Au_{38} nanoparticle melts were also measured over a range of temperatures; the thermal activation plots are shown in Figure 6, and the barrier energies ($E_{A,ET}$) are found in Tables 2 and 3.

TABLE 3: Voltammetric Measurements of Electron-Transfer Rate and Conductivity Measurements of Counterion Diffusion in Au_{38} Nanoparticle Polyether Melt (25 °C) with Added $MePEG_{550}$ (5:1) and 1 M $LiClO_4$ (Li^+/Ether Oxygen ≈ 1:16)[9b]

	CO_2 pressure (psi)				
measured parameter	vacuum	100	200	300	400
D_{APP} (25 °C)/10^{-8} cm^2 s^{-1}	0.84	1.61	1.92	2.27	2.97
k_{EX} (25 °C)/10^7 M^{-1} s^{-1}	1.15	2.38	2.84	3.37	4.40
$E_{A,ET}$/kJ mol^{-1}	50	38	34	28	22
D_{ClON} (2 5°C)/10^{-8} cm^2 s^{-1}	1.86	2.84	3.66	4.50	6.55
$E_{A,ClON}$/kJ mol^{-1}	56	43	38	34	24

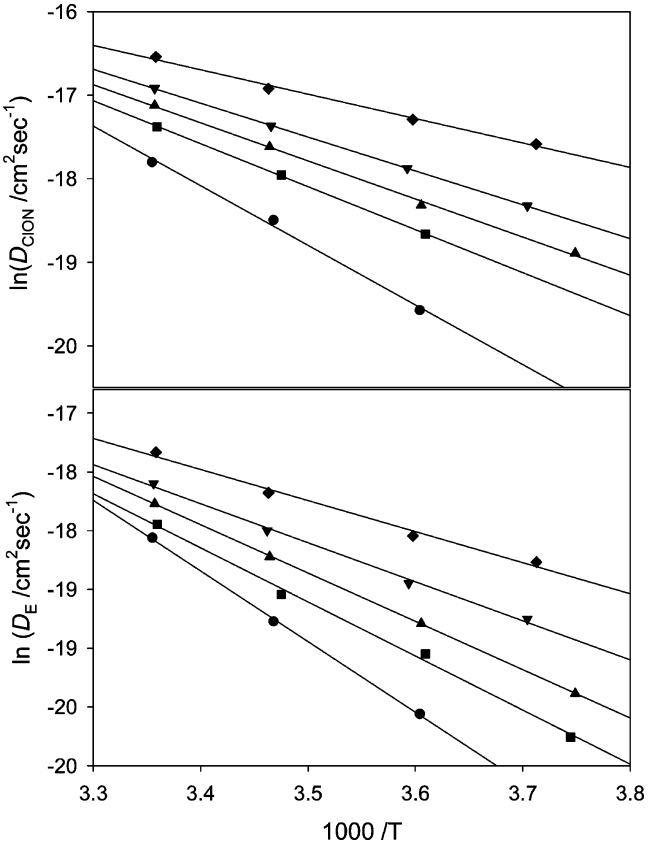

Figure 6. Thermal activation plots for D_{ClON} and D_E obtained in Au_{38} nanoparticle melts with added $MePEG_{550}$ (5:1) and 1 M $LiClO_4$ over the temperature range from −10 to 25 °C in a vacuum (●) and under CO_2 of 100 psi (■), 200 psi (▲), 300 psi (▼), and 400 psi (◆).

The rates of counterion transport in MePEG and CO_2-plasticized Au_{38} nanoparticle melts, containing ca. 1 M $LiClO_4$, were evaluated from ionic conductivity measurements (σ_{ION}) using the Nernst−Einstein equation as done previously[9b,25]

$$\sigma_{ION} = \frac{F^2}{RT}[z_{Li^+}{}^2 D_{Li^+} C_{Li^+} + z_{ClO_4^-}{}^2 D_{ClO_4^-} C_{ClO_4^-}] \qquad (2)$$

where z, D, and C are charge, diffusion coefficient, and concentration of the indicated species, respectively. Ionic conductivity in polymer electrolytes, and we assume also in the Au_{38} nanoparticle melt, mainly reflects the physical mobility of the ClO_4^- ion. Lithium ion transport in polyether solid electrolytes is known to be slowed by its interactions with PEG ether coordination sites.[9b,14] The diffusion coefficients of the perchlorate counterion (D_{ClO_4} or D_{ClON}) thus calculated from ionic conductivities, and the thermal activation barrier energies for ion transport ($E_{A,ClON}$) evaluated as in Figure 6, are listed in Tables 2 and 3.

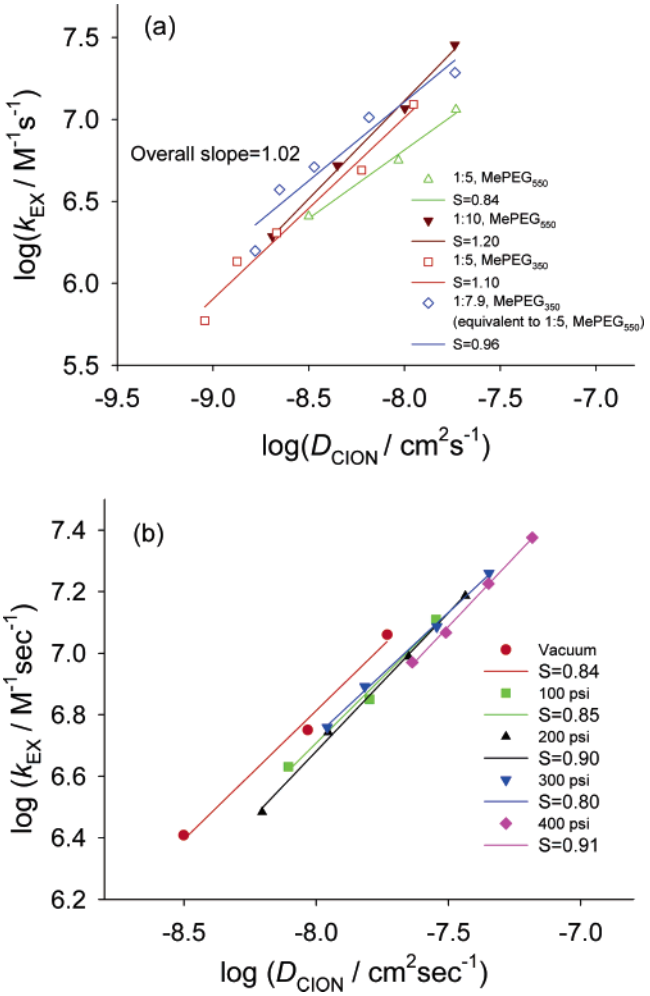

Figure 7. (a) Linear log−log relationship between k_{EX} and D_{CION} for $Au_{38}^{1+/0}$ electron transport in polyether melts with added different amounts of $MePEG_{350}$ or $MePEG_{550}$ over the temperature range from −10 to 25 °C in a vacuum. The average slope is 1.02. (b) Linear log−log relationship between k_{EX} and D_{CION} for $Au_{38}^{1+/0}$ electron transfer in Au_{38} polyether melts with added $MePEG_{550}$ (5:1) and 1 M $LiClO_4$ at a range of temperatures (−10 to 25 °C) in a vacuum and different CO_2 pressure.

Nature of Control of $Au_{38}^{1+/0}$ Electron Transfer Rate Constants. Inspection of the data in Tables 2 and 3 makes obvious that both the rates of electron hopping transport ($D_{APP} \approx D_E$) and counterion transport (D_{CION}), as reflected in their respective diffusion coefficients, and their activation barrier energies ($E_{A,ET}$ and $E_{A,CION}$) are very similar in numerical magnitude and in variation with the degree of MePEG or CO_2-induced plasticization. The largest plasticization-induced changes are in the barrier energies in Table 3, but they remain the same for $E_{A,ET}$ and $E_{A,CION}$, and the D_{APP} and D_{CION} values remain similar. The correlations in these data are accentuated by the Figures 7a and 7b log−log plots of k_{EX} and D_{CION}, where values of electron self-exchange rate constants linearly track their corresponding counterion diffusion coefficients, over different temperatures in melts plasticized with added $MePEG_{550}$ (5:1) and in room-temperature melts plasticized at different CO_2 pressures. The slopes are near unity, and the correlation extends over more than a 10-fold range. Tables 2 and 3 and Figures 7a and 7b strongly suggest that the rates of electron transfers between Au_{38}^0 and Au_{38}^{1+} cores are closely coupled to rates of counterion transport. It must be emphasized that the D_E and k_{EX} measurements are in a context of charge *transport*; that is, the rates obtained from $D_{APP} \approx D_E$ are solely the rates of transfer events that are fruitful in conveying electronic charge to and from the working electrode in the nanoparticle melt.

Correlations such as that in Figure 7 have been seen before, in the context of analogous charge and counterion transport investigations of polyether-based molten materials containing more conventional redox centers.[8,10] Our analysis of the coupling between electron and counterion transport uses a model termed *ion atmosphere relaxation*. The previous melts and the Au_{38} nanoparticle melts are highly viscous, amorphous media with high concentrations of electron donor−acceptor sites, the ionically charged ones of which are intrinsically contact ion-paired with their counterions owing to the absence of any substantial diluting solvent. The electrostatic consequences of the strong ion association can be expected to be larger than would be the case in dilute solutions with excess electrolyte present and where electrolyte ion mobility is furthermore much greater. The ion relaxation scheme, shown as a cartoon in Figure 8, can be written

$$ClO_4^-Au_{38}^+Au_{38}^0 \underset{k_{-1}}{\overset{k_1}{\rightleftharpoons}} ClO_4^-Au_{38}^0Au_{38}^+ \xrightarrow{k_2} Au_{38}^0Au_{38}^+ClO_4^-$$

where k_1 and k_{-1} are the forward and reverse electron transfer rate constants and k_2 is the rate constant for diffusive redistribution of the neighboring counterion(s). The counterion diffusion competes with the reverse electron transfer process; if it is slower (i.e., $k_2 \ll k_{-1}$), then most of the forward electron transfers are followed simply by reverse electron transfer. The electrochemical measurement measures charge *transport* and thus reflects only those events for which successful counterion relocation prevents back-electron transfer. The counterion diffusion rate thus controls transport of electrons by the electron transfer reaction. The overall rate constant (k_{EX}) can be written as

$$k_{EX} = \frac{k_1 k_2}{k_2 + k_{-1}} \approx \frac{k_1 k_2}{k_{-1}} = K_{EQ} k_2 \qquad (3)$$

where $K_{EQ} = k_1/k_{-1}$. The rate constant (k_2) for the diffusive counterion relocation rate constant can be modeled as[26]

$$k_2 = D_{CION}\left(\frac{\pi}{2a}\right)^2 \qquad (4)$$

where a is the diffusion distance.

Equations 3 and 4 lead to the conclusion that the apparent electron transfer rate constant (k_{EX}) should be proportional to the counterion diffusion coefficient (D_{CION}), just as seen in Tables 2 and 3 and Figure 7. Qualitatively, one would additionally expect that the rate k_2 should be increased by a larger concentration of counterions, relative to the nanoparticle concentrations, and some increase in k_2 with increase in the ratio C_{ClO_4}/C_{MPC} indeed can be seen in the Table 2 data (see right hand column). Variation of C_{ClO_4}/C_{MPC} was accomplished by varying the plasticizer content; the actual $LiClO_4$ concentration was not varied.[27]

No assumption is made in the above model regarding the chemical nature of the electron donor and acceptor sites, so the ion atmosphere model is quite general. The measured electron transfer rate constants k_{EX} are only apparent, not intrinsic values, being dominated by the slower rate of diffusive counterion relaxation to relieve the local charge imbalance. The generality of the ion atmosphere relaxation idea is emphasized by Figure 9, where the Au_{38} results are combined with analogous data from a variety of electron transfer reactions for other chemical

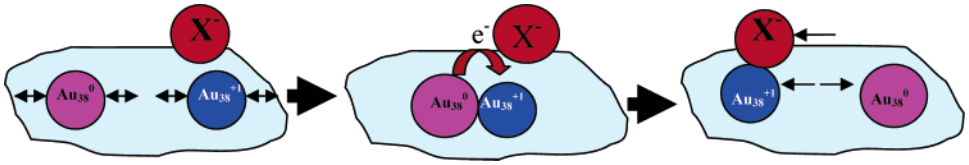

Figure 8. Cartoon of the electron transfer process controlled by ion atmosphere relaxation.

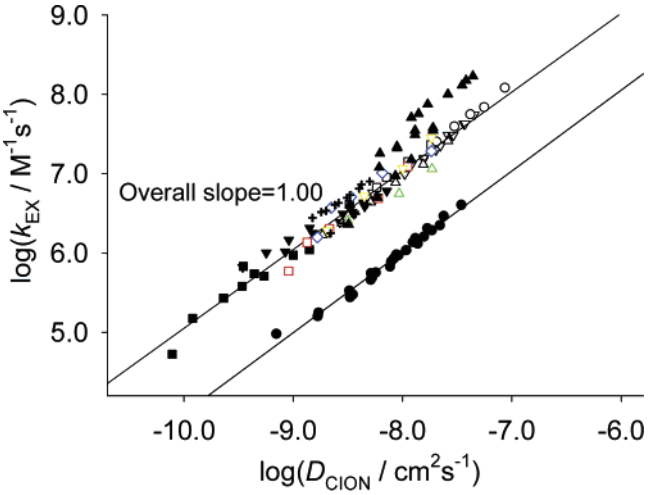

Figure 9. The data in Figure 7 coplotted with literature data from CO_2-plasticized melts, $[Co(phen)_3](MePEG_{350}SO_3)_2$[8b] (▽) and $[Co(bpy(CO_2MePEG_{350})_2)_3](ClO_4)_2$[8a] (▼), $MePEG_{350}$ plasticized melt $[Co(phen)_3](MePEG_{350}SO_3)_2$[8c] in molar ratios of 6:1 (○), 3:1 (□), and 2:1 (△) and $[Co(bpy(CO_2MePEG_{350})_2)_3]((ClO_4)_2 + xLiClO_4)$[9b] (■) ($x = 0-1.31$), $[Ru(bpy(CH_2MePEG_{350})_2)_2](CN)_2$ plasticized with CO_2 (over a range of temperatures)[8d] (●), $[Ru(bpy(CO_2MePEG_{350})_2)_3][X]_2$, where X = ClO_4^- or a mixture of ClO_4^- and I^- (+),[8e] and $[Cp_2Co](MePEG_{350}SO_3)$ melt (neat, $MePEG_{350}$ plasticized or mixed with $[FcTMA]^+$)[10] (▲). The overall slope for the linear correlation is 1.00.

species, including Co(II/I) bipyridine and phenanthroline complexes (PEGylated variously by attachment to the ligand or the counterion), Ru(III/II) bipyridine and cyano complexes, and cobalticinium/cobaltocene. The intrinsic electron transfer rate constants for these disparate couples must surely span a wide range of different values, but in the context of their reactions in semisolid melts that fruitfully yield electron *transport*, they all fall onto a common correlation line (except the Ru cyano case which is the only nonspherically symmetrical example and which has been discussed[8d]). The overall linear fitting gives an average slope of 1.00.

Let us finally examine the matter of the intercept of the correlated Au_{38} melt data. The intercept according to eqs 3 and 4 contains the equilibrium constant K_{EQ} and the diffusion distance a. Table 2 shows some calculations under different indicated assumptions. For an unselective reaction ($K_{EQ} = 1$), the calculated diffusion length a is smaller than the *average* center-to-center separation of the Au_{38} nanoparticles. If K_{EQ} is assumed to be less than unity (which is more reasonable given the unfavorable charge separation), then a is only about a nanometer. The actual distance at which electron transfer occurs thus seems to be smaller than the *average* center-to-center separation of the Au_{38} nanoparticles, an observation analogous to PEGylated metal complex melts where electron transport rates were independent of the polyether chainlength.[2c] The soft polyether shells certainly do not prevent neighboring Au nanoparticle cores, by thermal motions within the surrounding organic volume, from attaining smaller center-to-center separations. It is unclear, however, to what extent such thermal motion contributes to the energy barrier of electron transport and how it is related to the dynamics of counterion relaxation.

Acknowledgment. This research is supported in part by the National Science Foundation Science and Technology Center for Environmentally Responsible Solvents and Processes and by a grant from the Office of Basic Energy Sciences, Department of Energy. The authors gratefully acknowledge helpful conversations with Dr. Stephen Feldberg about this research during his Fall 2005 visit to UNC.

Supporting Information Available: Supplementary information on synthesis, voltammograms, and ^1H NMR spectra. This material is available free of charge via the Internet at http://pubs.acs.org.

References and Notes

(1) (a) *Polymer Electrolyte Reviews 1 and 2*; MacCallum, J. R., Vincent, C. A., Eds.; Elsevier Applied Science: London, 1987 and 1989. (b) Gauthier, M.; Fauteaux, D.; Vassort, G.; Belanger, A.; Duval, M.; Ricouxi, P.; Chabagno, J. M.; Muller, D.; Rigaud, P.; Armand, M. B.; Deroo, D. *J. Electrochem. Soc.* **1985**, *132*, 1333.

(2) (a) Surridge, N. A.; Sosnoff, C. S.; Schmehl, R.; Facci, J. S.; Murray, R. W. *J. Phys. Chem.* **1994**, *98*, 917. (b) Long, J. W.; Velazquez, C. S.; Murray, R. W. *J. Phys. Chem.* **1996**, *100*, 5492. (c) Williams, M. E.; Masui, H.; Long, J. W.; Malik, J.; Murray, R. W. *J. Am. Chem. Soc.* **1997**, *119*, 1997. (d) Masui, H.; Murray, R. W. *Inorg. Chem.* **1997**, *36*, 5118. (e) Emmenegger, F.; Williams, M. E.; Murray, R. W. *Inorg. Chem.* **1997**, *36*, 3146. (f) Kulesza, P. J.; Dickinson, E.; Williams, M. E.; Hendrickson, S.; Murray, R. W. *J. Phys. Chem. B* **2001**, *105*, 5833.

(3) (a) Williams, M. E.; Murray, R. W. *J. Phys. Chem. B* **1999**, *103*, 10221. (b) Dickinson, E.; Williams, M. E.; Hendrickson, S. M.; Masui, H.; Murray, R. W. *J. Am. Chem. Soc.* **1999**, *121*, 613.

(4) Leone, A. M.; Tibodeau, J. D.; Bull, S. H.; Feldberg, S. W.; Thorp, H. H.; Murray, R. W. *J. Am. Chem. Soc.* **2003**, *125*, 6784.

(5) Long, J. W.; Kim, I. K.; Murray, R. W. *J. Am. Chem. Soc.* **1997**, *119*, 11510.

(6) (a) Ito, K.; Ohno, H. *Electrochim. Acta* **1998**, *43*, 1247. (b) Ritchie, J.; Murray, R. W. *J. Phys. Chem. B* **2001**, *105*, 11523.

(7) Bard, A. J.; Faulkner, L. R. *Electrochemical Methods: Fundamental and Applications*, 2nd ed.; John Wiley & Sons: New York, 2001.

(8) (a) Lee, D.; Hutchison, J. C.; Leone, A. M.; DeSimone, J. M.; Murray, R. W. *J. Am. Chem. Soc.* **2002**, *124*, 9310. (b) Lee, D.; Harper, A. S.; DeSimone, J. M.; Murray, R. W. *J. Am. Chem. Soc.* **2003**, *125*, 1096. (c) Harper, A. S.; Lee, D.; Crooker, J. C.; Wang, W.; Williams, M. E.; Murray, R. W. *J. Phys. Chem. B* **2004**, *108*, 1866. (d) Ranganathan, S.; Murray, R. W. *J. Phys. Chem. B* **2004**, *108*, 19982. (e) Wang, W.; Lee, D.; Leone, A. M.; Murray, R. W. *Chem. Phys.* **2005**, *319*, 126.

(9) (a) Pyati, R.; Murray, R. W. *J. Am. Chem. Soc.* **1996**, *118*, 1743. (b) Williams, M. E.; Lyons, L. J.; Long, J. W.; Murray, R. W. *J. Phys. Chem. B* **1997**, *101*, 7584. (c) Williams, M. E.; Crooker, J. C.; Pyati, R.; Lyons, L. J.; Murray, R. W. *J. Am. Chem. Soc.* **1997**, *119*, 10249. (d) Dickinson V. E.; Masui, H.; Williams, M. E.; Murray, R. W. *J. Phys. Chem. B* **1999**, *103*, 11028.

(10) Harper, A. S.; Leone, A. M.; Lee, D.; Wang, W.; Ranganathan, S.; Williams, M. E.; Murray, R. W. *J. Phys. Chem. B* **2005**, *109*, 18852.

(11) (a) Schmid, G. *Inorg. Synth.* **1990**, *27*, 214. (b) Schaaff, T. G.; Shafigullin, M. N.; Khoury, J. T.; Vezmar, I.; Whetten, R. L.; Cullen, W. G.; First, P. N.; Gutierrez-Wing, C.; Ascensio, J.; Jose-Yacaman, M. J. *J. Phys. Chem. B* **1997**, *101*, 7885. (c) Brown, L. O.; Hutchison, J. E. *J. Am. Chem. Soc.* **1997**, *119*, 12384 (d) Chen, S.; Ingram, R. S.; Hostetler, M. J.; Pietron, J. J.; Murray, R. W.; Schaaff, T. G.; Khoury, J.; Alvarez, M. M.; Whetten, R. L. *Science* **1998**, *280*, 2098. (e) Hakkinen, H.; Barnett, R. N.; Landman, U. *Phys. Rev. Lett.* **1999**, *82*, 3264.

(12) (a) Donkers, R. L.; Lee, D.; Murray, R. W. *Langmuir* **2004**, *20*, 1945. (b) Lee, D.; Donkers, R. L.; DeSimone, J. M.; Murray, R. W. *J. Am. Chem. Soc.* **2003**, *125*, 1182. (c) Lee, D.; Donkers, R. L.; Wang, G.; Harper, A. S.; Murray, R. W. *J. Am. Chem. Soc.* **2004**, *126*, 6193.

(13) (a) Guo, R.; Song, Y.; Wang, G.; Murray, R. W. *J. Am. Chem. Soc.* **2005**, *127*, 2752. (b) Guo, R.; Murray, R. W. *J. Am. Chem. Soc.* **2005**, *127*, 12140.

(14) (a) Watanabe, M.; Itoh, M.; Sanui, K.; Ogata, N. *Macromolecules* **1987**, *20*, 569. (b) Watanabe, M.; Nagano, S.; Sanui, K.; Ogata, N. *Polym. J.* **1986**, *18*, 809. (c) Wooster, T. T.; Watanabe, M.; Murray, R. W. *J. Phys. Chem.* **1992**, *96*, 5886.

(15) The Au_{38} after the ligand-exchange reaction with PEGylate thiols is sparingly soluble in nonpolar solvent (e.g., heptane).

(16) Pale-Grosdemange, C.; Simon, E. S.; Prime, K. L.; Whitesides, G. M. *J. Am. Chem. Soc.* **1991**, *113*, 12.

(17) Templeton, A. C.; Hostetler, M. J.; Kraft, C. T.; Murray, R. W. *J. Am. Chem. Soc.* **1998**, *120*, 1906.

(18) PEGylated ligand-protected Au_{38} nanoparticles are soluble in a relatively polar solvent such as acetonitrile, in which $Au_{38}(PhC2)_{24}$ is insoluble. The change of solubility is, in part, evidence for the ligand exchange reaction.

(19) Conway, B. E.; Angerstein-Kozlowska, H.; Sharp, W. B. A.; Criddle, E. E. *Anal. Chem.* **1973**, *45*, 1331.

(20) (a) Dubois, D.; Moninot, G.; Kutner, W.; Jones, M. T.; Kadish, K. M. *J. Phys. Chem.* **1992**, *96*, 7137. (b) Evans, D. H.; Hu, K. J. *J. Chem. Soc., Faraday Trans.* **1996**, *92*, 3983. (c) Roth, J. D.; Lewis, G. J.; Safford, L. K.; Jiang, X.; Dahl, L. F.; Weaver, M. J. *J. Am. Chem. Soc.* **1992**, *114*, 6159. (d) Franceschetti, A.; Zunger, A. *Phys. Rev. B* **2000**, *62*, 2614.

(21) Choi, J. P. University of North Carolina, Chapel Hill, NC. Unpublished data, 2005.

(22) (a) Dahms, H. *J. Phys. Chem.* **1968**, *72*, 362. (b) Ruff, I.; Friedrich, V. J. *J. Phys. Chem.* **1971**, *75*, 3297. (c) Majda, M. In *Molecular Design of Electrode Surfaces*; Murray, R. W., Ed.; John Wiley & Sons: New York, 1992.

(23) (a) Sullenberger, E. F.; Michael, A. C. *Anal. Chem.* **1993**, *65*, 2384. (b) Dressman, S. F.; Michael, A. C. *Anal. Chem.* **1995**, *67*, 1338.

(24) The Table 3 data, and those given below for counterion transport in CO_2-plasticized melts, may underestimate the degree of transport enhancement since we were unable to ascertain the degree of melt swelling (and change in Au_{38} concentration) caused by the CO_2 sorption. The unswollen concentration, 3.14×10^{-2} M, was employed. Previously[5a] induced CO_2 swelling of a polyether-based metal complex melt was ca. 10% at 400 psi.

(25) MacCallum, J. R.; Vincent, C. A. *Polymer Electrolyte Reviews*; Elsevier Applied Science: Oxford, U. K., 1987; Vol. 1.

(26) Marcus, R. A. *J. Phys. Chem. B* **1998**, *102*, 10071.

(27) Plasticizer concentration and CO_2 pressure were varied in the present study, but the concentration of $LiClO_4$ electrolyte was not. Previous results[9b] show that changes in $LiClO_4$ concentration produce complex changes in the fluidity (viscosity) of redox PEG melts and the diffusivity of ions therein. Decrease in $LiClO_4$ concentration actually increases ionic conductivity, for example, owing to the coordinative cross-linking effect of Li^+ ions with ether oxygens. Nonetheless, previous charge and ion transport data taken[9b] at varied $LiClO_4$ concentrations do follow the generalized pattern of ion atmosphere relaxation in $[Co(bpy(CO_2MePEG_{350})_2)_3]$ $(ClO_4)_2$ melts, and such data are included in Figure 9.